

Waves of constant shape and the structure of the “rotors boundary” in excitable media.

Yu.E. Elkin¹, V.N. Biktashev^{1,2,*} & A.V. Holden³

May 22, 2001

¹ *Institute for Mathematical Problems in Biology, Pushchino, Moscow Region, 142292, Russia*

² *Department Mathematical Sciences, University of Liverpool, Liverpool L69 9ZL, UK*

³ *Department of Physiology, University of Leeds, Leeds LS2 9JT, UK*

* *Author to whom correspondence should be addressed*

Abstract

We classify possible fixed-shaped excitation wave patterns in \mathbb{R}^2 , in terms of the kinematic approach. These patterns include rotating waves (diverging and converging spiral waves), and translating waves (retracting waves, “critical fingers” and “V-shaped” patterns). We analyze regions of existence of these patterns in the parametric space, and compare the results with those obtained by numerical simulations and with the “free-boundary” approach.

1 Introduction.

Propagating waves are observed in different physical, chemical and biological excitable media [1, 2, 3, 4]. One of the most important applications is the analysis of the spiral waves of excitation which underlie dangerous cardiac arrhythmias [5].

The kinematic approach is an approximation used for the description of propagation of excitation waves following one after another at large intervals [6, 7, 8]. It exploits the fact that the main factor determining the wave propagation velocity is the local curvature of the wave, which provides the equation of motion of the wave as a curve (in 2D) or a surface (in 3D). In the case of a broken wave, it is necessary to supplement this equation by boundary conditions at the wave break (tip) and by tip motion equations.

The kinematic approach is ideologically close to the so called free boundary approach [9] in that both consider movement of lines; the crest line of the wave for the former, and the front/back line for the latter. However, the conditions of applicability are different, and the description is made in different terms. For instance, the kinematic approach may be applicable even in the case when there is no sharp wavebacks, as is the case with cardiac excitation equations, or even no sharp wavefronts. Another difference is the absence of

the concept of the wave break in the free boundary approach, while it plays an important role in the kinematic approach. So translation from one language to the other may be not straightforward or even not always possible.

There are cases, however, when both approaches can be applied and the results are comparable. Such is the case of the “universal limit” of large-core spiral waves in the free-boundary approach [10, 11, 12]. The properties of solutions there correspond to the phenomenological boundary of existence of spiral waves (rotors) ∂R by Winfree [13]. The kinematic approach of [8] also considered a boundary of existence of spiral wave solution, also hypothetically identified with ∂R . However, the phenomenological properties of the kinematic solutions were different, which created an apparent contradiction between the kinematic approach on one hand, and the free-boundary approach, and, to a certain extent, the numerical simulations, on the other hand.

In this paper we study the properties of the solutions in the kinematic approach in more detail, and eliminate the above mentioned contradiction. Briefly, the result is that the boundary of existence of spiral wave solutions consists of two different analytical branches, and [10, 11, 12] dealt with one branch while [8] was considering the other branch.

We describe a variety of fixed-shape excitation wave patterns in the vicinity of the boundary of existence of spiral wave solutions. These patterns may execute translational (translating waves) or rotational (spiral waves) movement and they exist on different sides of this boundary. For the sake of completeness, we present all such solutions, including those known earlier. We describe the dependence of the shapes and kinematical parameters of the patterns on medium parameters, and regions of existence of different patterns in the parametric space. The results agree with those of the free-boundary approach [10, 11, 12]. The present results are more complete, in the sense that variations of parameters are considered which are not expressible in terms of the free-boundary theory. Of course, the question of realisability of these parameters in any particular reaction- diffusion system remains open, as the parameters of the kinematic description cannot be obtained analytically and have not been yet obtained numerically. This remains a question for future study.

The structure of the paper is as follows. In section 2 we introduce essential ideas and equations of kinematic approach. In sections 3 and 4 we present solutions in the form of translating and rotating waves. Finally, in section 5 we compare our results with results of free boundary approach.

2 Kinematic approach.

The kinematic approach is based on the curvature-velocity dependence [6, 7, 8] for the normal velocity of wave propagation, V_n , and curvature of the wave, K :

$$V_n(s, t) = V_* - DK(s, t) \tag{1}$$

where K is considered positive if the wave is convex in the direction of propagation, s is arclength along the wave measured from the tip of the wave, and V_* and D are parameters

of the medium. From now on we will use dimensionless variables:

$$l = V_* D^{-1} s, \quad \kappa = D V_*^{-1} K. \quad (2)$$

A wave of stationary shape obeys the equation [6, 7]

$$\kappa' = \kappa \left(\int_0^l \kappa(1 - \kappa) dl - \gamma \right) - \Omega. \quad (3)$$

Here $\gamma = G/V_*$ is the dimensionless and G is the dimensional tip shrink rate, *i.e.* the component of the tip velocity along the tangent to the wave; $\Omega = D V_*^{-2} \omega$, ω is rotation frequency for spiral wave and $\omega = 0$ for translating waves. In the case of small curvature $\kappa \ll 1$, equation (3) can be brought to the form

$$\kappa \kappa'' - \kappa'^2 - \kappa^3 - \Omega \kappa' = 0 \quad (4)$$

The boundary condition as s tends to infinity is

$$\kappa(\infty) = 0 \quad (5)$$

and boundary conditions at the tip were formulated in [8]. Their dimensionless form for the case of small $\kappa \ll 1$, $\Omega \ll 1$ and $\kappa'(0) \ll \kappa(0)$ may be presented as

$$\kappa(0) = \epsilon; \quad \gamma \epsilon + \kappa'(0) + \Omega = 0. \quad (6)$$

Dimensionless parameters ϵ and γ are the only two parameters of the medium in this approximation. In this paper we assume them both to be small, $\epsilon \ll 1$, $\gamma \ll 1$. Note that tip shrink rate is

$$\gamma = G/V_* = -(\kappa'(0) + \Omega)/\kappa(0). \quad (7)$$

So, equation (4) with boundary conditions (5), (6) poses the problem for the unknown function $\kappa(l)$ and unknown number Ω . Solutions of this problem with $\Omega \neq 0$ correspond to the rotating waves while solutions with $\Omega = 0$ are the translating waves.

3 Translating waves.

Here we consider the case $\Omega = 0$. Phase portraits of equations (3) and (4) at $\Omega = 0$ are presented on Fig. 1.

Figure 1 near here

General solutions of (4) with $\Omega = 0$ are

$$\kappa_0(l) = 2/(l + A)^2 \quad (8)$$

$$\kappa_-(l) = -2A_1^2 / \cosh^2(A_1 l + A_2^-) \quad (9)$$

$$\kappa_+(l) = 2A_1^2 / \sinh^2(A_1 l + A_2^+) \quad (10)$$

$$\kappa_p(l) = 2A_1^2 / \cos^2(A_1 l + A_2) \quad (11)$$

with arbitrary integration constants A, A_1, A_2^\pm, A_2 . These solutions have been discussed e.g. in [14, 15]. Thus, for $\epsilon = 0$ the problem (4,5,6) has only the solution in the form of a plane broken wave $\kappa = 0$. Below we consider $\epsilon \neq 0$.

All solutions $\kappa_{0\pm}$ satisfy boundary condition at infinity (5). Their plots in (l, κ) plane and shapes of corresponding waves are presented on Fig. 2.

Figure 2 near here

Solution (11) does not satisfy the boundary condition (5). Moreover, for this solution $\kappa_p \gg 1$ when $A_1 l + A_2 \rightarrow \pi/2$, and hence (4) is not a valid approximation for (3). Some parts of such solutions can be used to construct appropriate solutions in piece-wise media, see also [15, 16, 17]. Furthermore, when critical curvature is introduced, the loops in 3(b) convert into cusps [18], what makes such solutions tractable in the context of the trigger waves, for which the kinematic theory can be also applied. Following this predution of the kinematic theory, the corresponding solutions have been constructed for PDE models in [19, 20]. For completeness, we present a numerical solution of equation (3), corresponding to a closed phase trajectory on Fig. 3.

Figure 3 near here

We will call solution κ_- a concave wave and solution κ_+ a convex wave, in accordance with convexity or concavity of the wave line in the direction of movement, and solution κ_0 a logarithmic wave, for reasons which will be clear later.

Arbitrary constants in solutions $\kappa_{0\pm}$ may be obtained from the boundary conditions (6):

$$\begin{aligned} A &= 2/\gamma, \quad A_1 = \frac{1}{2} (\gamma^2 - 2\epsilon)^{1/2}, \\ \tanh A_2^- &= \coth A_2^+ = \frac{\gamma}{(\gamma^2 - 2\epsilon)^{1/2}}, \end{aligned} \quad (12)$$

with

$$\gamma^2 \geq 2\epsilon \quad (13)$$

required for existence of translating waves.

The arbitrary constants and the region of existence for solution (11) are

$$A_1 = \frac{1}{2} (2\epsilon - \gamma^2)^{1/2}, \quad \tan A_2 = -\frac{\gamma}{(2\epsilon - \gamma^2)^{1/2}} \gamma^2 < 2\epsilon. \quad (14)$$

One can see from phase portrait on Fig. 1, that the translating waves are concave waves κ_- if $\kappa(0) < 0$ and logarithmic waves κ_0 or convex waves κ_+ (if they exist) if $\kappa(0) > 0$. The logarithmic wave κ_0 corresponds to the equality in (13), and the convex wave κ_+ to the strong inequality. Note that solutions κ_0 and κ_+ can satisfy boundary conditions at infinity (5) only if $\kappa'(0) < 0$. Then, by (7), since $\Omega = 0$ and $\kappa(0) > 0$, we conclude that in this case $\gamma > 0$. Taking into account the boundary conditions (6), the regions of existence of translating waves of different types can be summarised as:

$$\kappa = 0 \quad : \quad \epsilon = 0 \quad (15)$$

$$\kappa_0 \quad : \quad \gamma^2 = 2\epsilon, \quad \gamma > 0 \quad (16)$$

$$\kappa_- \quad : \quad \epsilon < 0 \quad (17)$$

$$\kappa_+ \quad : \quad \gamma^2 \geq 2\epsilon, \quad \gamma > 0 \quad (18)$$

Conditions (16) and (18) imply that logarithmic waves κ_0 and convex waves κ_+ are always shrinking and never growing, while concave waves κ_- and plane waves $\kappa = 0$ may be both shrinking or growing.

The wave line shape in Cartesian coordinates can be obtained from natural equations (8)–(10) via

$$\begin{aligned} \phi(l) &= \int_0^l k_n(\xi) d\xi, \\ x(l) &= \int_0^l \cos(\phi(\xi)) d\xi, \\ y(l) &= \int_0^l \sin(\phi(\xi)) d\xi \end{aligned} \quad (19)$$

Hence the asymptotics, for $l \rightarrow \infty$, of our solutions are

$$\begin{aligned} y_0 &\sim \text{const} + 2 \ln x \\ y_{\pm} &\sim \tan(2A_1)x. \end{aligned} \quad (20)$$

This is why we called solution κ_0 a logarithmic wave. Note that asymptotics (20) coincide with those of the retracting waves and the critical finger solution of [11]. Solution κ_- with no wavebreaks coincides with the V-shaped patterns described in [21].

4 Spiral waves.

Phase portraits for equations (3) and (4) for $\Omega \neq 0$ are shown on Fig. 4. The difference between the phase portraits is insignificant if κ and κ' are small.

Figure 4 near here

Solutions corresponding to the phase trajectories on the right of the separatrix AO on Fig. 4b reach infinite curvature in finite length and hence do not satisfy boundary condition at infinity (5). Corresponding trajectories on Fig. 4a do not go to infinity, but the curvature becomes very large, $\kappa \ll 1$, *i.e.* the kinematic approach is not formally applicable. For completeness, we illustrate the shape of these “curly spiral” solutions in Fig. 5.

Figure 5 near here

There are two different types of solutions which satisfy boundary condition at infinity (5). Some solutions pass through point I at Fig. 4 to the left half-plane, and the curvature becomes negative. This means that far from the tip, the waves propagate towards the center of rotation, rather than from it. We will call these patterns convolving spirals. Note that such patterns in a bounded medium have been observed in numerical simulation [22]. An example of such a solution and the corresponding wave shape are presented on Fig. 6(b,b'). Another type of solution is the separatrix AO on the phase portrait. In contrast to the previous type, this solution is positive everywhere and will be called evolving spiral. The graph of $\kappa(l)$ and wave shape for this solution are shown on Fig. 6(a,a'). In subsequent discussion, we consider evolving spirals only, *i.e.* we replace the boundary condition at infinity (5) by a more restrictive one:

$$\kappa(+\infty) = +0 \tag{21}$$

Figure 6 near here

All solutions of equation (4) can be described analytically[8] (see also [23] for a related solution in terms of Airy functions). It is convenient to do so in a piecewise manner:

$$\begin{aligned} \kappa(l) &= \pm(9/2)^{1/3}\Omega^{2/3}\zeta^{2/3}(1 \pm Y^2(\zeta)), \\ \zeta &= \frac{\sqrt{2}}{3}\Omega^{1/2}|l_0 - l|^{3/2}, \end{aligned} \tag{22}$$

where for $l \leq l_0$ we choose upper signs and

$$Y(\zeta) = \frac{qJ_{-2/3}(\zeta) - J_{+2/3}(\zeta)}{J_{-1/3}(\zeta) + qJ_{+1/3}(\zeta)}, \tag{23}$$

and for $l \geq l_0$ we choose lower signs and

$$Y(\zeta) = \frac{I_{+2/3}(\zeta) - qI_{-2/3}(\zeta)}{I_{-1/3}(\zeta) - qI_{+1/3}(\zeta)}, \quad (24)$$

and where l_0 and q are integration constants; $J_p(x)$ and $I_p(x)$ are Bessel functions and modified Bessel functions respectively. We will call these pieces the J -branch and the I -branch respectively; note that one is the analytical continuation of the other. These solutions satisfy boundary condition (21) only when $q = 1$. Solutions with $q < 1$ correspond to the convolving spirals, and those with $q > 1$ correspond to the phase trajectories on the right of the separatrix. Spirals of different types can be used to construct piecewise solutions in inhomogeneous media [24].

The tip point ($l = 0$) may be on the J -branch if $l_0 > 0$ (J -type spiral wave) or on the I -branch if $l_0 < 0$ (I -type spiral wave). The infinite tail of the spiral is described by the I -branch in all cases. So J -type spirals consist of two pieces, the J -branch at the tip and the I -branch in the rest, while I -type spirals are of I -branch everywhere.

From (6), the boundary conditions at the tip for J -type and I -type spirals are

$$\begin{aligned} \pm \frac{6^{2/3}}{2} (1 \pm Y_0^2) \zeta_0^{2/3} \Omega^{1/3} &= \epsilon \\ 3(1 \pm Y_0^2) \zeta_0 \Omega^{1/2} Y_0 &= -\gamma \epsilon \end{aligned} \quad (25)$$

where $Y_0 = Y(\zeta_0)$, $\zeta_0 = \sqrt{2\Omega}/3 \cdot |l_0|^{3/2}$ and $Y(\zeta)$ is the corresponding function from (23) or from (24).

Thus, the problem of finding the spiral wave solution is reduced to the finite transcendental system (25) with respect to ζ_0 and Ω . Other kinematical parameters of the spiral wave can be expressed through these two quantities. In particular, the core radius r_0 and the angle between the wave tangent at the tip and the direction from the rotation center to the tip α are

$$r_0 = [(1 - \epsilon)^2 + \gamma^2]^{1/2} / \Omega, \quad \tan \alpha = \gamma / (1 - \epsilon). \quad (26)$$

Solution of (25) is

$$\Omega = \pm \frac{1}{(6\zeta_0)^2} (2\epsilon - \gamma^2)^3 \quad (27)$$

where ζ_0 is the least positive root of the equation $Y_0 = Y(\zeta_0)$ with $Y(\zeta)$ from (23) or (24) and

$$Y_0 = \mp \frac{\gamma}{(\pm(2\epsilon - \gamma^2))^{1/2}} \quad (28)$$

Upper or lower signs, and hence J - or I - type of the spiral, are taken so that the expression in right-hand side of (28) is real, so that J -spirals exist if

$$\gamma^2 - 2\epsilon < 0 \quad (29)$$

and I -spirals exist if

$$\gamma^2 - 2\epsilon > 0. \quad (30)$$

In the latter case, there is an additional necessary condition. Since the boundary conditions at infinity (21) can be only satisfied at $q = 1$, and this implies that $Y(\zeta) < -1$ ¹. Hence we can see from (24) that

$$\gamma < 0, \quad \epsilon > 0. \quad (31)$$

Comparing (31) with (7) we can see that I -spirals may only be growing, while J -spirals can be both growing or shrinking.

Finally, note that the existence regions of I - and J -type solutions with $q \neq 1$ are described by inequalities (29)–(31) respectively, as well as those for corresponding I - and J -type evolving spirals.

5 Conclusion.

Although the solutions with large curvatures and self-intersections might be of interest in terms of motion of abstract curves, they are of limited interest in the context of excitation waves, as the high curvatures violate the applicability of the kinematic approximation, and excitation waves in all known excitable media strongly interact with each other and cannot be superimposed. The existence regions for other types of solutions are summarised on Fig. 7. One can see that regions of existence of translating and rotating waves exactly complement each other, *i.e.* there are no gaps and no overlaps between them.

Figure 7 near here

Boundaries between regions “J” and “C” (J/C -boundary) and between “I” and “V” (I/V -boundary) separate regions of spiral and translating waves. In particular, the J/C -boundary may be identified with Winfree’s phenomenological rotor boundary ∂R [13] and the boundary between spiral and retracting waves as described in [12].

Compare the dependency of the translating wave shrink rate on the distance δ to the J/C -boundary in the parametric space, when this distance is small, for our “convex waves” and “retracting waves” in the free-boundary theory. First of all, definitions of shrink rates in the present study and in [10, 11, 12] are different. Here it is the projection of the tip velocity on *the wave tangent at the tip*; hereafter this will be referred to as the local shrink rate. And in [10, 11, 12] the shrink rate was its projection on *the asymptotical direction of the wave far from the tip*. We will call this the global shrink rate. We use the symbol G for the local shrink rate, and denote the global shrink rate by G^{glob} . The global shrink rate may be expressed through the local shrink rate as

$$G^{glob} = G \cos \Phi - V_n \sin \Phi \quad (32)$$

¹Indeed, if $q = 1$ then $Y = -K_{2/3}(\zeta)/K_{1/3}(\zeta)$. By Sommerfeld’s integral representation, $K_\nu(\zeta) = \int_0^\infty \exp(-\zeta \cosh \psi) \cosh(\nu \psi) d\psi > 0$ and if $\nu > 0$ then $\partial_\nu K_\nu(\zeta) = \int_0^\infty \psi \exp(-\zeta \cosh \psi) \sinh(\nu \psi) d\psi > 0$. Therefore, $K_{2/3}(\zeta) > K_{1/3}(\zeta) > 0$ and $Y = -K_{2/3}(\zeta)/K_{1/3}(\zeta) < -1$ as required.

where $V_n = V_*(1 - \kappa(0))$ is the normal tip velocity and $\Phi = \phi(\infty)$ is the total orientation angle change along the wave. By denoting $\delta = \epsilon - \gamma^2/2$, we obtain for our solutions:

$$\begin{aligned} G_0^{glob}/V_* &= O(\gamma^2) \\ G_+^{glob}/V_* &= (-2\delta)^{1/2} + O(\delta\gamma, \delta^{3/2}). \end{aligned} \quad (33)$$

These asymptotics agree for small γ , and coincide for $\gamma = 0$, with those presented in [10]: $G = 0$ for a “critical finger” and $G \propto \delta^{1/2}$ for “retracting waves”. So we can say that our convex waves solutions κ_+ can be identified with the “retracting waves” of the free-boundary theory and the logarithmic wave κ_0 is identical with the “critical finger” of that theory.

For concave waves solutions κ_- the boundary of existence region is line $\gamma = 0$ and distance to this boundary in parametric space is $-\epsilon$. The global shrink rate of concave waves in the vicinity of the point ($\gamma = 0$, $\epsilon = 0$) is

$$G_-^{glob}/V_* = (-2\epsilon)^{1/2} + O(\gamma^2, \epsilon). \quad (34)$$

Finally, using the asymptotics of Bessel functions, we can obtain asymptotics of the rotation frequency Ω from (27) near the J/C -boundary:

$$\Omega \approx \frac{\sqrt{2}}{3\zeta_*} \delta^{3/2} \quad (35)$$

where ζ_* is the smallest positive root of equation $Y(\zeta_*) = 0$ and Y is from (23). Asymptotic estimate (35) coincides with that obtained in [25, 12]: $\Omega \propto \delta^{3/2}$.

Summarising, we can point out features of translating waves and rotating spiral waves in an excitable medium, which are identical to the corresponding features in the free boundary approach [10, 11, 12]:

- There exists the J/C -boundary, a manifold of codimension 1 in the medium parameters space, at which there exist translating waves of a “logarithmic shape” (logarithmic waves/critical fingers).
- On one side from J/C -boundary, there exist spiral waves only but not translating waves.
- On the other side there are no rotating spiral waves, but there are translating waves (convex/retracting waves). The asymptotical shape of the convex/retracting waves is linear.
- The global tip growth rate, *i.e.* the tip velocity projection on the direction of the far from the tip, for the logarithmic wave/critical finger equals zero.
- The global tip growth rate of the convex/retracting waves decreases with the distance $\delta \rightarrow 0$ to the J/C -boundary in parametric space as $\propto \delta^{1/2}$.

- On the other side of the J/C boundary, the rotation frequency of the spiral waves decreases with $\delta \rightarrow 0$ as $\propto \delta^{3/2}$.

In [8], the vicinity of the line $\epsilon = 0$ was considered, implying also $|\gamma| \sim 1$. This is the I/V boundary on the diagram Fig. 7. The properties of the rotating and translating waves around this boundary are partly similar and partly different from those of J/C boundary (here we assume $|\gamma| \ll 1$):

- The I/V -boundary is also a manifold of codimension 1 in the medium parameters space. At this manifold, there exist translating solutions in the form of broken, asymptotically linear, rather than logarithmic, waves.
- Similarly to the J/C boundary, on one side from I/V -boundary, there exist spiral waves only but not translating waves. However, the spiral waves are of I -type rather than J -type.
- Similarly to the J/C boundary, on the other side there are no rotating spiral waves, but there are asymptotically linear translating waves. However, these translating waves are concave rather than convex.
- The global tip growth rate, *i.e.* the tip velocity projection on the direction of the far from the tip, for the broken linear waves on the I/V boundary is zero, similarly to the J/C boundary.
- The retraction rate changes with the distance δ to boundary in parametric space (which for the I/V -boundary can be identified with $|\epsilon|$): $\propto |\epsilon|^{1/2}$, similarly to J/C -boundary.
- On the other side of the I/V boundary, the rotation frequency of the spiral waves is $\propto \delta$, rather than $\propto \delta^{3/2}$.

For details of the relevant solutions, see [8]. As some of the properties of these solutions do not have counterparts in the free-boundary theory, these can be considered as a *new prediction of the kinematic theory*.

As the derivation of the kinematic equations in [6, 7, 8] was based on very general considerations of symmetry and stability, and also on the assumptions of existence of a certain type of solution, which was never directly verified, the question about observability of I/V boundary in real reaction-diffusion equations is not obvious. It is clear, however, that if this behaviour is to be observed, this would *not* be in a FitzHugh-Nagumo type system with disproportion of the excitation and recovery times, with excitation pulses having sharp backs and sharp fronts, as such systems are covered by the free-boundary theory. And since most of the well-studied models of excitable systems belong to this class, this may explain why this behaviour has not been observed so far. Alternative examples of excitable systems are known. A simple three-component excitable system with sharp fronts but smooth backs has been proposed as early as 1972 [26], and it is well known that equations of cardiac excitability produce excitation pulses with sharp fronts but not with sharp backs.

Acknowledgments

Authors are grateful to V. Hakim and A. Karma for stimulating discussions, and to anonymous referees for bibliographical advice. The work was supported in parts by Robert Havemann Foundation (Y.E.E.) and by the Wellcome Trust (V.N.B).

References

- [1] H. L. Swinney and V. I. Krinsky. Waves and patterns in chemical and biological media (*special issue*). *Physica D*, 49:1–255, 1991.
- [2] A. V. Holden, M. Markus, and H. G. Othmer, editors. *Nonlinear wave processes in excitable media*. Plenum, New York, 1991.
- [3] J. Brindley and P. Gray. Nonlinear phenomena in excitable media (*special issue*). *Phil. Trans. Roy. Soc. Lond. ser. A*, 347:599–727, 1994.
- [4] A. V. Holden and M. S. El Naschie. Nonlinear phenomena in excitable physiological systems (*special issue*). *Chaos Solitons and Fractals*, 5:317–726, 1995.
- [5] R. A. Gray and J. Jalife. Spiral waves and the heart. *Int. J. Bifurcation and Chaos*, 6(3):415–435, 1996.
- [6] V. A. Davydov, V. S. Zykov, and A. S. Mikhailov. Kinematics of autowave patterns in excitable media. *Sov. Phys. Uspeki*, 161:45–86, 1991.
- [7] A. S. Mikhailov, V. A. Davydov, and V. S. Zykov. Complex dynamics of spiral waves and motion of curves. *Physica D*, 70:1–39, 1994.
- [8] Yu. E. Elkin, V. N. Biktashev, and A. V. Holden. On the movement of excitation wave breaks. *Chaos Solitons and Fractals*, 9:1597–1610, 1998.
- [9] J. J. Tyson and J. P. Keener. Singular perturbation theory of traveling waves in excitable media (a review). *Physica D*, 32:327–361, 1988.
- [10] A. Karma. Velocity selection in two-dimensional excitable media: from spiral waves to retracting fingers. In M. B. Amar *et al.*, editor, *Growth and Form*. Plenum, New York, 1991.
- [11] A. Karma. Universal limit of spiral wave propagation in excitable media. *Phys. Rev., Lett.*, 66:2274–2277, 1991.
- [12] V. Hakim and A. Karma. Spiral wave meander in excitable media: the large core limit. *Phys. Rev., Lett.*, 79:665–668, 1997.
- [13] A. T. Winfree. Varieties of spiral wave behaviour — an experimentalist’s approach to the theory of excitable media. *Chaos*, 1:303–334, 1991.

- [14] A. Mulholland and J. Gomati. The eikonal approximation to excitable reaction-diffusion systems: Travelling non-planar wave fronts on the plane. *Physica D*, 89:329–345, 1996.
- [15] P. Brazhnik. Exact solutions for the kinematic model of autowaves in two-dimensional excitable media. *Physica D*, 84:205–220, 1996.
- [16] J. Tyson and P. Brazhnik. Propagation of waves through a line of discontinuity in two-dimensional excitable media: Refraction and reflection of autowaves. *Phys. Rev., E*, 54:1958–1968, 1996.
- [17] J. Tyson and P. Brazhnik. Steady-state autowave patterns in a two-dimensional excitable medium with a band of different excitability. *Physica D*, 102:300–312, 1997.
- [18] J. Tyson and P. Brazhnik. Nonspiral excitation waves beyond the eikonal approximation. *Phys. Rev., E*, 54:4338–4346, 1996.
- [19] J. Tyson and P. Brazhnik. Travelling waves and static structures in a two-dimensional exactly solvable reaction-diffusion system. *J. Phys. A*, 32:8033–8044, 1999.
- [20] J. Tyson and P. Brazhnik. On traveling wave solutions of Fisher’s equation in two spatial dimensions. *SIAM J. Appl. Math.*, 60(2):371–391, 1999.
- [21] P. K. Brazhnik and V. A. Davydov. Non-spiral autowave structures in excitable media. *Phys. Lett. A*, 199:40–44, 1995.
- [22] O. A. Mornev, O. V. Aslanidi, and Chaylakhyan L. M. Soliton regime in FitzHugh-Nagumo equations: dynamics of rotating spiral wave. *Sov. Phys. Doklady*, 353:682–686, 1997.
- [23] H. Yamada and K. Nozaki. Dynamics of wave fronts in excitable media. *Physica D*, 64:153–162, 1993.
- [24] A. Voford, P.L. Simon, H. Farkas, and Z. Nosticius. Rotating chemical waves: theory and experiments. *Physica A*, 274:30–49, 1999.
- [25] V.A. Davydov, A.S. Mikhailov, and P. Brazhnik. A kinematical approach to the description of autowave processes in active media. *Theor.Math.Phys.*, 74:440–447, 1988.
- [26] E. C. Zeeman. Differential equations for the heartbeat and nerve impulse. In C. H. Waddington, editor, *Towards a Theoretical Biology — an IUBS symposium*, volume 4: Essays. Edinburgh University Press, Edinburgh, 1972.

Figure captions

Figure 1. (a) Phase portrait of equation (4) with $\Omega = 0$. The separatrix solution (8) and two members of every family (9)–(11) are shown. The phase plane is separated by bold lines, the axis κ' and the separatrix κ_0 , into four regions with different behaviour of solutions. On the right of the separatrix are solutions κ_p of the form (11). These solutions reach infinite curvature in finite length, and thus can not satisfy boundary condition at infinity (5). On the left of κ' -axis are concave wave solutions κ_- (9). They start from the point $\kappa = 0, \kappa' = 0$ at $l = -\infty$ and return to this point at $l = +\infty$. Finally, between the κ' -axis and the separatrix, are the convex wave solutions κ_+ (10). Their behaviour is similar to that of the separatrix solution, *i.e.* phase trajectories go from infinity to the point $\kappa = 0, \kappa' = 0$, when l runs from $-A_2^+/A_1^+$ (or $-A$ for κ_0) to $+\infty$ (lower part) or go from this point to infinity when l runs from $-\infty$ to $-A_2^+/A_1^+$ ($-A$ for κ_0) (upper part). (b) Phase portrait of equation (3) for comparison. The difference is insignificant for small κ and κ' . For large $\kappa > 0$ trajectories of (3) are closed, while trajectories of (4) go to infinity.

Figure 2. Curvature vs arclength for translating waves: (a) $\kappa_0(l)$ (8) for $\epsilon = 0.1$, (b) $\kappa_+(l)$ (10) for $\epsilon = 0.1, \gamma = 0.5$, and (c) $\kappa_-(l)$ (9) for $\epsilon = -0.1, \gamma = 0.5$. The corresponding wave shapes are shown on panels (a') – (c'). The tips are marked by the points on the lines, the dotted lines are the analytical continuations of the wave lines through the tips. The arrows show the direction of the wave propagation.

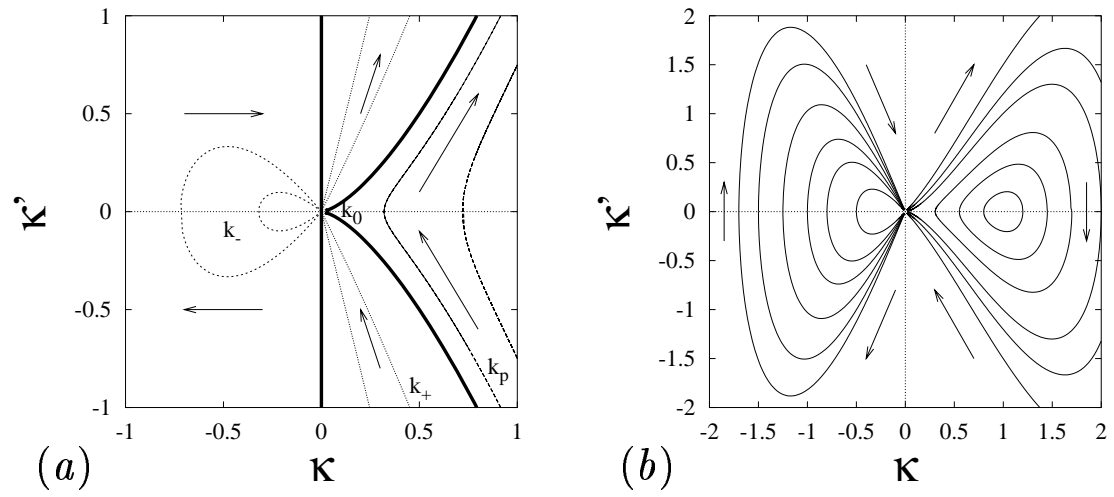
Figure 3. (a) Curvature vs arclength for the numerical solution of (3,6) $\Omega = 0, \epsilon = 0.01$ and $\gamma = 0$. (b) The corresponding wave shape. The tip is marked by the point on the line, the dotted line is the analytical continuation of the wave line through the tip. The arrow shows the direction of the wave propagation. Self-intersection of the wave line means this wave shape, although being a formal solution to the corresponding ODEs, cannot be observed in a real excitation wave, and the high curvature in the loops means the kinematic approximation is not valid.

Figure 4. (a) Phase portrait of equation (3) with $\Omega = 0.5$ in coordinates $(\kappa\Omega^{-2/3}, \kappa'\Omega^{-1})$. (b) Phase portrait of equation (4) in coordinates $(\kappa\Omega^{-2/3}, \kappa'\Omega^{-1})$. O is a complex equilibrium, I is a non-equilibrium singular point. Bold solid line AO is the separatrix of the origin.

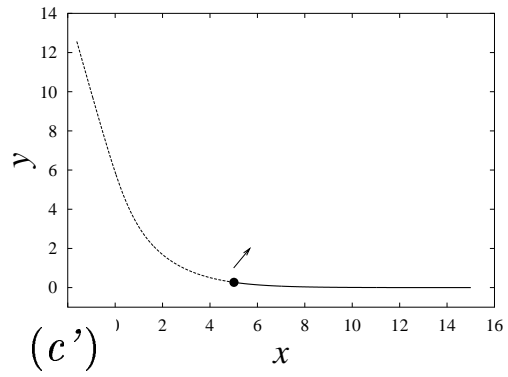
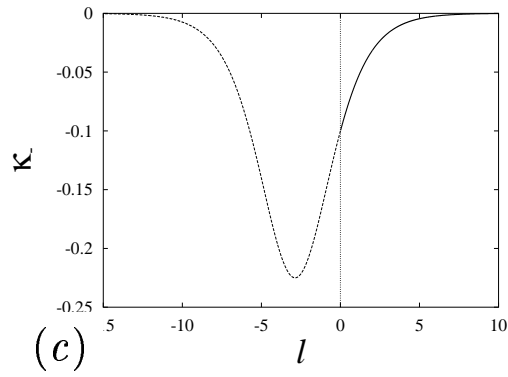
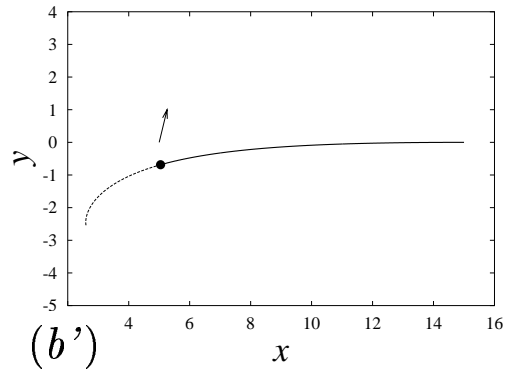
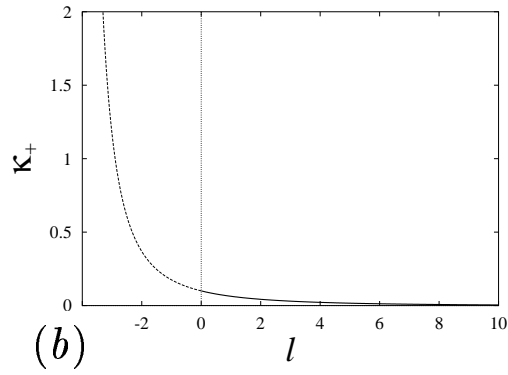
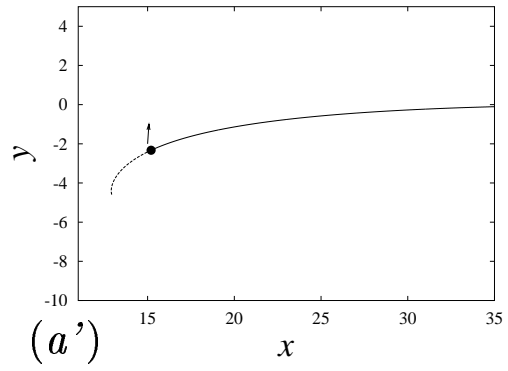
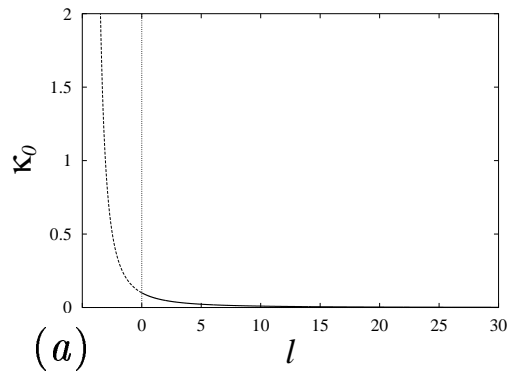
Figure 5. (a) Curvature vs arclength for a “curly spiral” solution with $\Omega = 0.005, \epsilon = 0.2, \gamma = 0.35$. (b) Its wave line shape. Spiral rotates in counterclockwise direction, as shown by arrows. Rotation center is at origin. Tip is shown by point. Dashed circle is the tip trajectory. (c) Magnified view of dashed rectangle on (b). Self-intersection of the wave line means this wave shape, although being a formal solution to the corresponding ODEs, cannot be observed in a real excitation wave, and high curvature in the loops means the kinematic approximation is not valid.

Figure 6. Curvature vs arclength for (a) evolving and (b) convolving (sink) spirals and (a',b') shape of their wave lines. Both spirals rotate counterclockwise (shown by arrows) around the origin. The tips are shown by points. Dashed circles are the tips trajectories. Parameters of spirals are: (a) $\epsilon \approx 0.13$, $\gamma \approx -0.67$, $\Omega = 0.1$ (b) $\epsilon = 0.19$, $\gamma = -0.89$, $\Omega = 0.2$. (a'',b''): magnified views of dashed rectangles on (a') and (b'). Evolving spiral (a) was obtained from analytical solution (22), while convolving spiral (b) is the result of numerical integration of equation (3)

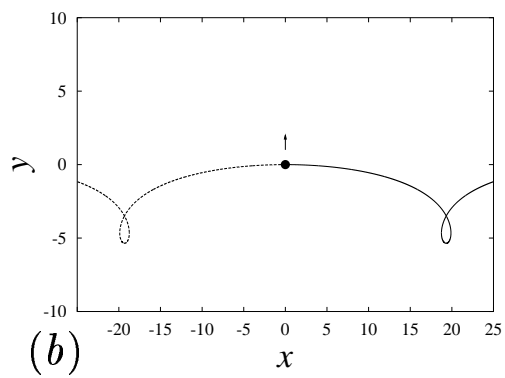
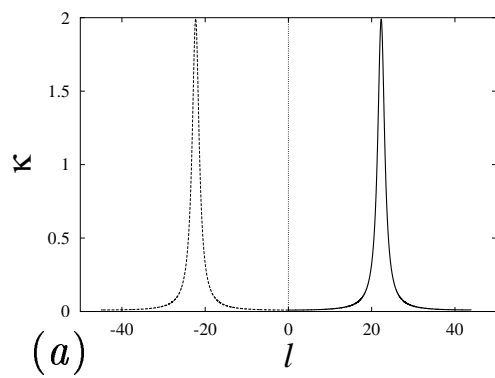
Figure 7. Existence regions for spiral and translating waves in the (ϵ, γ) -plane. Solid lines are boundaries between the regions. Bold line separates regions of rotating (*I* and *J*) and translating (*C* and *V*) waves. In region “*J*” where (29) fulfilled, *J*-type spiral waves exist. Region “*I*” is defined by conditions (30), (31). In this region *I*-type spiral waves exist. Region “*C*” is defined by conditions (18). In this region convex translating waves (10) exist. In region “*V*” where $\epsilon < 0$, concave translating waves (9) (“*V*-shaped waves”) exist. In addition at the boundary of “*J*” and “*C*” regions, logarithmic waves (8) exist, and at the line $\epsilon = 0$ half-plane waves exist.



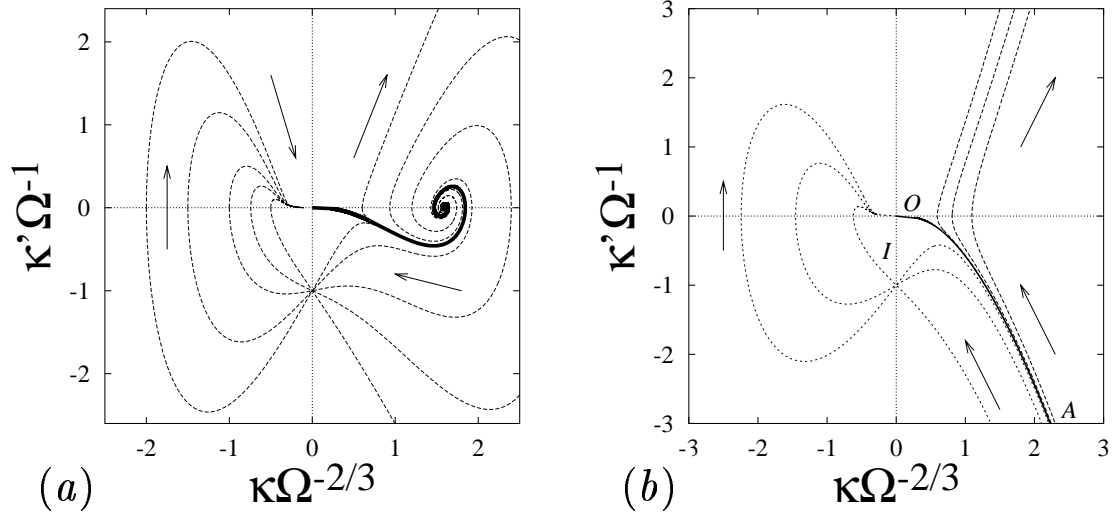
Y.E. Elkin, V.N. Biktashev and A.V. Holden
Waves of constant shape and the structure of the "rotors boundary" in excitable media.
Figure 1



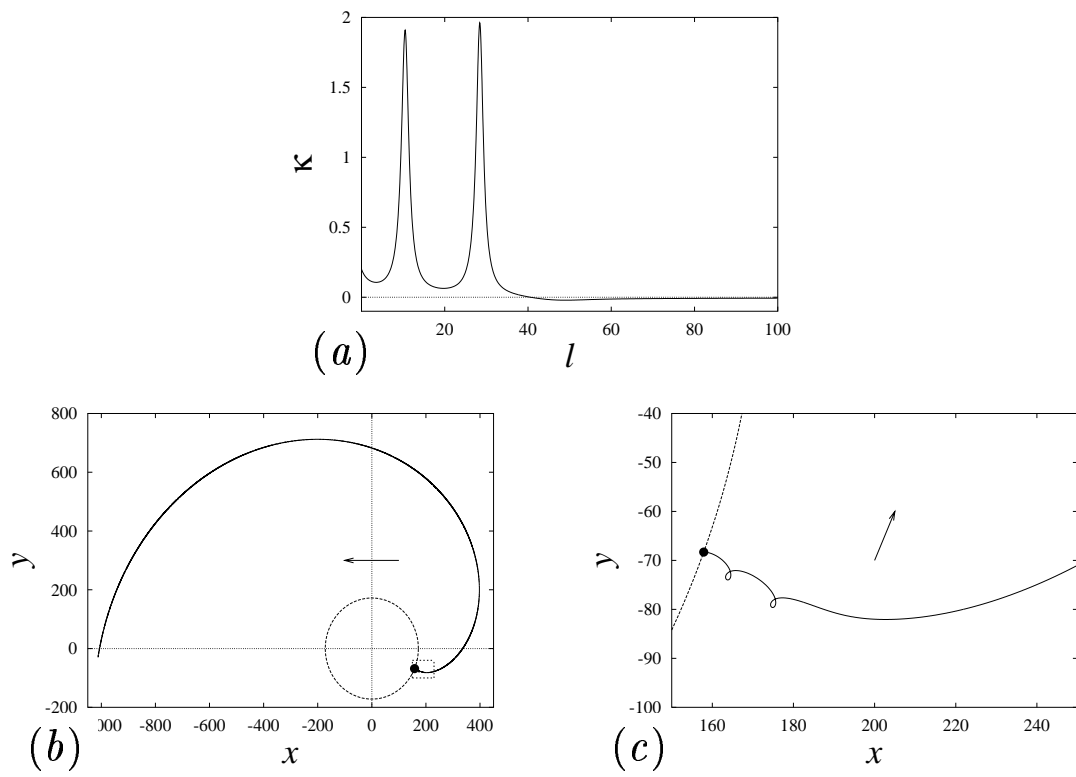
Y.E. Elkin, V.N. Biktashev and A.V. Holden
Waves of constant shape and the structure of the “rotors boundary” in excitable media.
Figure 2



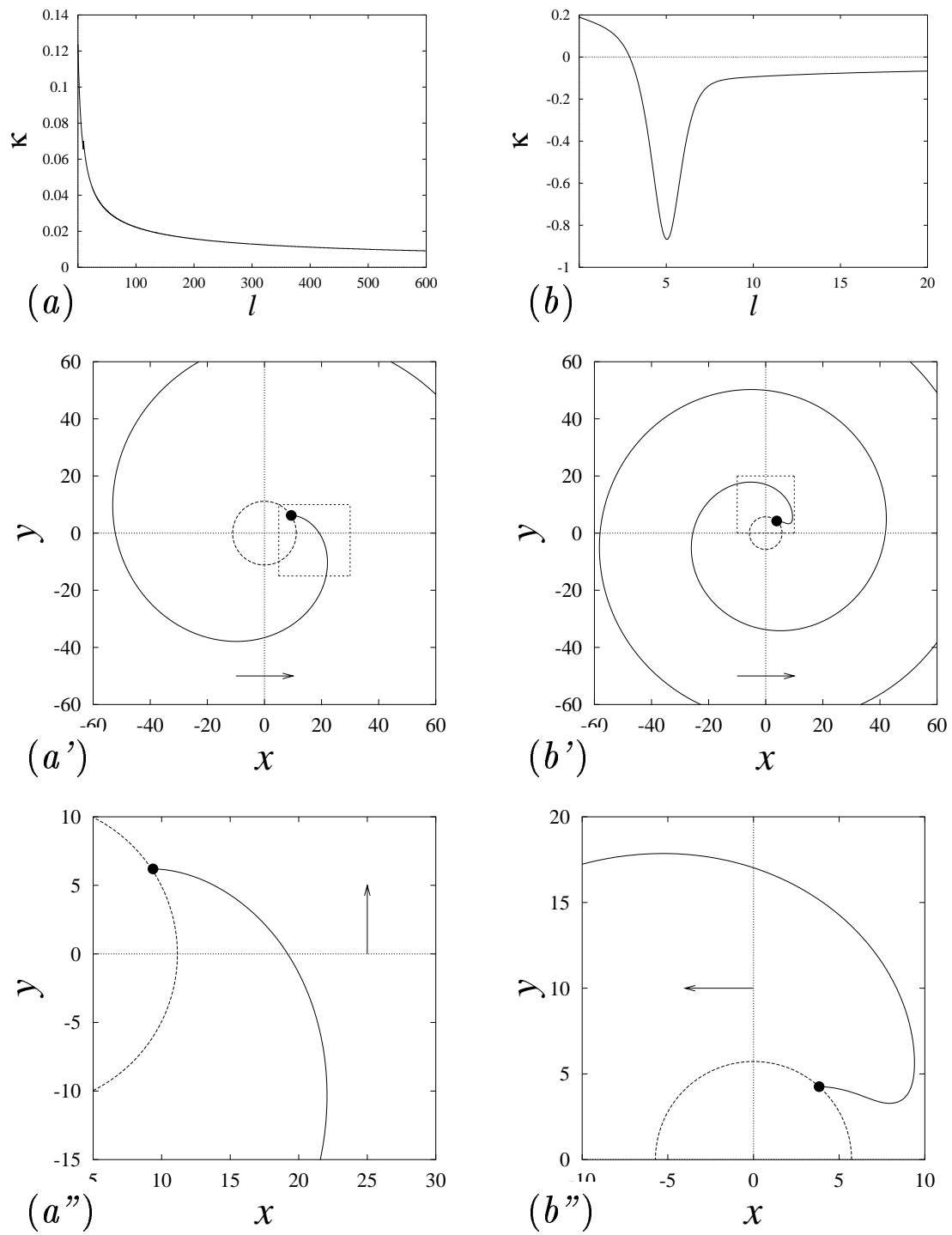
Y.E. Elkin, V.N. Biktashev and A.V. Holden
Waves of constant shape and the structure of the “rotors boundary” in excitable media.
Figure 3



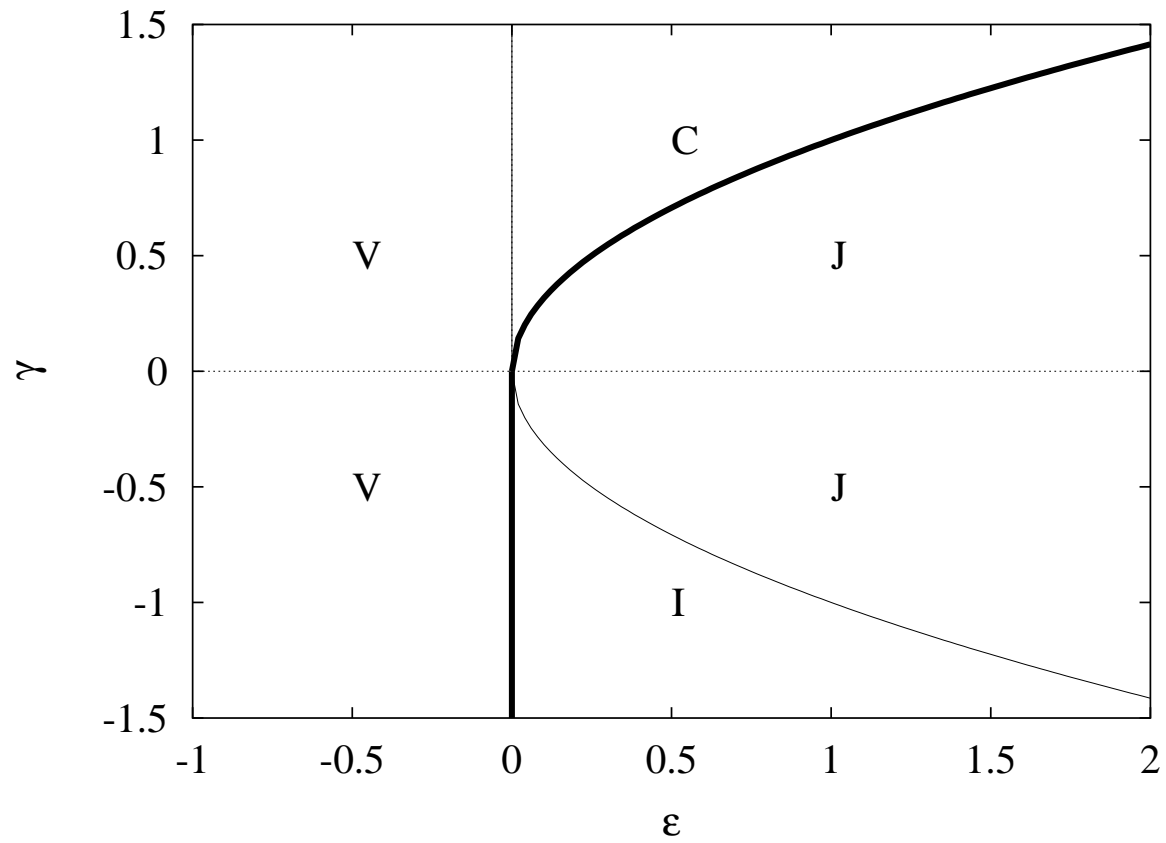
Y.E. Elkin, V.N. Biktashev and A.V. Holden
Waves of constant shape and the structure of the “rotors boundary” in excitable media.
Figure 4



Y.E. Elkin, V.N. Biktashev and A.V. Holden
Waves of constant shape and the structure of the “rotors boundary” in excitable media.
Figure 5



Y.E. Elkin, V.N. Biktashev and A.V. Holden
Waves of constant shape and the structure of the “rotors boundary” in excitable media.
Figure 6



Y.E. Elkin, V.N. Biktashev and A.V. Holden
Waves of constant shape and the structure of the “rotors boundary” in excitable media.
Figure 7